Bringing prospective motion correction to clinical routine - fast camera calibration

Cris Lovell-Smith[1], Julian Maclaren[2], Michael Herbst[1], Ilja Kadashevich[3], KA Danishad[3], Oliver Speck[3], and Maxim Zaitsev[1]
[1]*Department of Radiology, University Medical Center Freiburg, Freiburg, Germany,* [2]*Department of Radiology, Stanford University, Stanford, California, United States,* [3]*Faculty of Natural Sciences, Institute of Experimental Physics (IEP), Magdeburg, Germany*

TARGET AUDIENCE This abstract is targeted at those using an external tracking device for prospective motion correction.

PURPOSE The use of an optical tracking system to prospectively compensate for head movement during brain imaging has been shown to reduce motion artefacts [1, 2]. To successfully apply motion correction, the cross-calibration transform between tracking system coordinates and scanner coordinates must be accurately known. Previous methods to determine this transform [1] required two experienced MR technicians upward of 20 minutes to perform. We present two newly developed methods that accurately calculate the cross-calibration within two minutes with one operator, thereby reducing the system setup time considerably. This is a major step in bringing prospective motion correction to clinical routine.

The tracking system in this research is the moiré phase tracking system (MPT) [3] (Metria Innovation Inc., U.S.A) and comprises a camera and retro-reflective tracking markers. The MPT produces 6 degrees-of-freedom positional information for markers within the camera's field-of-view. A marker is attached to the patient's head during motion correction enabled measurements and the imaging volume is updated in accordance with the measured head movement.

METHODS We name our first new method "fixed marker recalibration". A tracking marker was fixed inside the bore of a Siemens 3T Trio (Siemens Healthcare, Germany) such that the patient table could move freely in and out of the bore over the top of the marker. The camera was attached to the top of the bore facing the patient table (Fig. 1).

Using the iterative method in Ref. 1 an accurate calibration was found. Following this the table was moved outside the scanner and the pose (position and orientation) of the marker (p_{saved}) and the camera calibration transform (T_{saved}) were recorded. The camera was then moved and recalibration using the fixed marker method tested. The recalibration algorithm uses the fact that the scanner coordinates were accurately defined using the fixed marker pose (p_{saved}) and the previous calibration matrix (T_{saved}). This information is exploited to find the new calibration transform (T_{new}) using the new measured marker pose (p_{new}). Here p_{saved} and p_{new} are defined in camera coordinates.

We define $T[p]$ as the transformation of the pose p from camera coordinates to scanner coordinates (here we use affine transform matrices, for rotation matrices, quaternions, and vectors the equations must be altered accordingly). We note that $T_{saved}[p_{saved}] = T_{new}[p_{new}]$ (Eq. 1), i.e. the pose of the fixed marker is a constant in the scanner coordinate system. All quantities except T_{new} are known allowing the equation to be rearranged and solved.

We named the second method "phantom recalibration". A spherical MR phantom was designed and printed using rapid prototyping technology. The phantom comprises an outer spherical shell and a complex pseudo-random 3D grid structure within (Fig 2). The inner structure was designed to yield 3D images with fairly homogenous spin density but without rotational symmetry allowing changes in phantom pose to be uniquely determined with a volume regisctration algorithm [4]. The grid was designed without sharp edges to reduce the chances of trapping air, and improve its registration properties. Attached to the surface of the phantom is an MPT tracking marker. Like the first method, an initial calibration is performed. The phantom is then scanned using a short 3D gradient echo sequence (TA = 90 s, 96 x 96 x 96 voxels, 2 mm isotropic). The scan data along with the pose of the marker attached to the phantom (p_{saved}), and the calibration matrix (T_{saved}) are stored.

The constant transform between the phantom's internal structure and the attached marker is exploited during recalibration. We define $T_{phantom}$ as the transformation the phantom undergoes from the reference scan to the recalibration scan, calculated by volume registration of the 3D structure between the two scans. We can then extend Eq. 1 to $T_{saved}[p_{saved}] = T_{phantom}^{-1}[T_{new}[p_{new}]]$ (Eq. 2), and solve for T_{new}. Applying the inverse transform $T_{phantom}^{-1}$ has the effect of returning the phantom to its initially scanned position in the bore thereby transforming the problem into the fixed marker calibration.

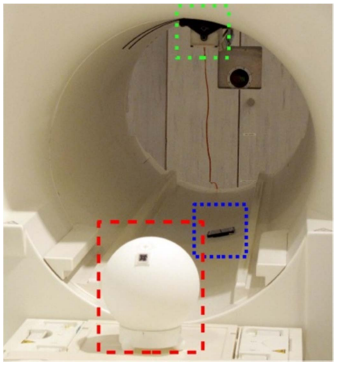

Fig. 1: The camera (green box) was mounted at the top of the bore, and the fixed marker was attached to the floor of the bore (blue box). The calibration phantom is shown in the foreground (red box). Both the phantom and the fixed marker allow the camera cross-calibration to be calculated.

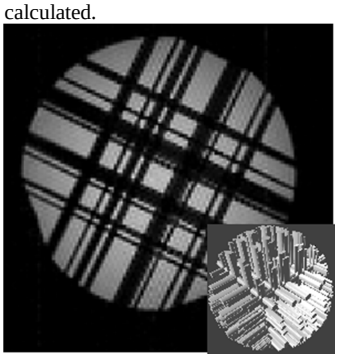

Fig. 2: Camera recalibration is accomplished using a spherical phantom with complex internal structure (inset bottom right) that facilitates volume registration, used during the calibration procedure. The MR image shows a cross section of the grid.

RESULTS To analyse the performance of the two methods, Ref. 1 was used to initially calibrate the system. Following this the calibration was saved using both of the presented methods. The camera was then moved seven times and each time the new calibration was calculated using all three methods. The positional and angular errors were defined for each method as the differences between the calibration gained using Ref. 1 and the new method in question. In this way the Ref. 1 method produced the ground truth transforms. For the positional error the Euclidean distance between the translation components of the transform was used. For the angular error the angular difference between the orientations was used. To estimate the error in the ground truth the difference between the transforms produced in the last two iterations of the method was used. The root mean square errors (RMS) were calculated by combining all seven data points and are shown in Table 1.

	Translational error (mm)	Angular error (degrees)	Duration (min:s)
Iterative cal. (Ref. 1)	0.429	0.134	20:00
Fixed marker recal.	0.594	0.255	0:10
Phantom recal.	1.394	0.215	1:30

Table 1: The two proposed methods were compared to the original 'iterative' calibration method (Ref. 1). The iterative calibration was considered the ground truth when calculating the accuracy of the two new methods. The values show the root mean square (RMS) errors in both the translation components and the angular components.

DISCUSSION & CONCLUSION Both methods perform well with errors comparable to the iterative method, however both new methods rely on the ground truth calibration and therefore the overall calibration accuracy will be a function of the errors in both the initial calibration and the methods themselves. By improving the initial calibration the new methods will likely also perform better. The reason for the greater phantom recalibration translation error is yet unknown however this accuracy is generally sufficient. Initial results at 7T are promising and will follow at a later date.

Both the presented methods complement each other. Fixed marker recalibration may become the 'every-day' calibration method due to its simplicity and speed, and phantom recalibration could be used as a fall-back procedure in case the fixed marker is moved or damaged. It also has the advantage of portability between same-model Siemens scanners, meaning a calibration can be saved at one scanner and then used to recalibrate another system (however the accuracy may be lower). The execution times are excellent but could be reduced further by averaging fewer poses during fixed marker recalibration, and by optimising the reference scan protocol used by the phantom recalibration. The accuracy of all three methods may be improved by optimising scan protocols to improve the performance of the volume registration algorithm. Finally both methods can be used to seed the iterative calibration method reducing the time to complete a new initial calibration.

Recalibration using these methods reduces the system-setup time considerably. A recalibration can be performed in under 2 minutes using either of the new methods described, resulting in at least a 10-fold reduction in calibration time. In a time-constrained clinical routine setting this is an extremely important step forward for prospective motion correction. In our setting the new methods allow us to install the camera on a clinical MR scanner on a patient-by-patient basis.

REFERENCES [1] Zaitsev et al, NeuroImage 31:038-1050. [2] Maclaren et al., DOI10.1002/mrm.24314. [3] Maclaren et al., PLOS ONE 2012. [4] Thesen et al., MRM 2000 Sep; 44(3):457-65.